Annals of Nuclear Energy 202 (2024) 110451

Contents lists available at ScienceDirect

Annals of Nuclear Energy

journal homepage: www.elsevier.com/locate/anucene

Itô-calculus based mathematical models for stochastic nuclear reactor kinetics and dynamics simulations of low neutron source nuclear power plant (NPP) start-up

T.L. Gordon [a,*], M.M.R. Williams [a], M.D. Eaton [a], P. Haigh [b]

[a] Nuclear Engineering Group, Department of Mechanical Engineering, City and Guilds Building, Exhibition Road, Imperial College London, South Kensington Campus, SW7 2BX, United Kingdom

[b] Rolls-Royce PLC, PO BOX 2000, Derby DE21 7XX, United Kingdom

ARTICLE INFO

Dataset link: https://zenodo.org/records/10776943

Keywords:
Caliban fast burst nuclear reactor
Cumulative Distribution Function (CDF)
Itô-Calculus
Pál-Bell
Wait-time Probability Distribution Function (PDF)

ABSTRACT

This paper investigates the effect thermal feedback has on the stochastic nuclear reactor dynamics of low neutron source nuclear power plant (NPP) start-ups. Stochastic mathematical and computational models are required to determine the probability of a stochastic power surge occurring during nuclear reactor start-up that would damage the nuclear fuel. The aim is to design the nuclear reactor, the nuclear fuel, and the operational start-up procedures in a manner that minimises the probability of a stochastic power surge occurring, which damages the nuclear fuel, to a prescribed level of probabilistic risk (10^{-8}–10^{-5}). Recently, the Pál-Bell equations have been used for such low neutron source nuclear reactor start-up simulations. However, the stochastic nuclear reactor start-up models, based upon the Pál-Bell equations, cannot accommodate changes in the macroscopic neutron cross-sections arising from feedback processes. An alternative approach that could, in principle, include thermal feedback processes is the forward master equations. However, these are complex to implement for multidimensional and multi-group stochastic nuclear reactor dynamics problems. In addition, time-dependent analog Monte Carlo models could be used but these are computationally prohibitive for most nuclear reactor start-up simulations. This is due to the stringent requirements on the statistical accuracy of the safety probability associated with stochastic power surges. Therefore, this paper uses an alternative Itô-calculus approach to compute the stochastic properties required for low neutron source NPP start-up. The Itô-calculus approach is an approximate mathematical method, compared to the more general Pál-Bell and Monte Carlo methods, for low neutron source nuclear reactor start-up and fast burst systems. Therefore, the implementation of the Itô calculus method is first validated against the Caliban fast burst nuclear reactor experimental wait-time results to understand the accuracy of the method. The implementation of a simple feedback model is also verified against the point neutron kinetics equations. The neutron population CDF calculated using the Pál-Bell equations without thermal feedback, and the safety probabilities computed with, and without, including thermal feedback mechanisms are then analysed and assessed. These results demonstrate that the Itô-calculus approach can be used to gain useful insight into the behaviour of stochastic nuclear kinetics and dynamics during low neutron source NPP start-up. Furthermore, the results suggest that the safety probabilities computed using the Pál-Bell method are not affected by neglecting thermal feedback mechanisms which is an important result from a nuclear reactor safety perspective.

1. Introduction

Accurate scalar neutron flux measurements must be constantly observed during Nuclear Power Plant (NPP) start-up (Schultz, 1955; Harrer, 1963; Harris, 1964; Williams, 1974). Source, intermediate, and power range neutron detectors, which have overlapping sensitivity ranges, help prevent the nuclear reactor from being taken super-critical without the operator's knowledge (Boland, 1970; Harrer and Beckerley, 1973, 1974; Tucker, 2019). When starting up for the first time, or after a prolonged shutdown period, the intrinsic neutron flux inside the nuclear reactor core might not exceed the lower end of the neutron flux detectors. In such a case, the control rods must be incrementally withdrawn until the neutron flux exceeds the functional range of the

* Corresponding author.
E-mail address: travis.gordon14@imperial.ac.uk (T.L. Gordon).

https://doi.org/10.1016/j.anucene.2024.110451
Received 2 November 2023; Received in revised form 11 January 2024; Accepted 22 February 2024

detection instruments. Withdrawing the control rods without accurate measurements indicating the change in the neutron flux is known as a 'blind start-up' and is always avoided if possible (Schultz, 1955; Harrer, 1963; Shaw, 1969; Lewis, 1977). Neutron sources are installed into the reactor core to maintain an accurate measurement of the scalar neutron flux. These neutron sources generate a large number of overlapping neutron chains, which help to maintain a continuous neutron detector reading. Power and temperature transients may then be calculated using deterministic methods if the neutron source strength is large enough. However, the primary and secondary neutron sources used for NPP start-up are costly (Martin et al., 2000) and present a radioactive hazard for construction workers (Shimazaki et al., 2016).

Therefore, it is advantageous to reduce the quantity of neutron source material involved during NPP start-up. However, reducing the neutron source strength introduces the need for mathematical and computational models of stochastic nuclear reactor kinetics and dynamics. Low neutron densities exhibit large fluctuations from the mean due to the inherently stochastic nature of neutron interactions with matter (fission and capture). While other sources of nuclear reactor noise exist, such as local fluctuations in coolant temperature, localised bubble formations or fuel/control rod vibrations, this study is only concerned with the noise arising from the inherently stochastic nature of nuclear fission and neutron capture in low neutron numbers.

The stochastic models required must be capable of accurately modelling low neutron densities and their associated fluctuations from the mean population. They must also be able to accurately compute the probability distribution function (PDF) or similarly the cumulative distribution function (CDF) of the neutron population at any prescribed instant in time (Hurwitz, 1959; Hurwitz et al., 1963b,a; MacMillan and Storm, 1963).

Multiple mathematical methods are capable of producing the neutron population CDF for a single neutron energy group system, namely the forward master equations (Harris, 1958; Hurwitz, 1959; Bell et al., 1963; MacMillan, 1970), the backward master equations (Pál-Bell) (Pál, 1958; Bell, 1965; Williams and Eaton, 2017, 2020), Monte-Carlo (Gang, 2011; Cooling et al., 2016; Sutton et al., 2017), and Itô-calculus (Allen, 2007, 2010).

An NPP start-up code called NDT3, which solved the forward master equations, was developed by Bell et al. (1963). MacMillan (1970) later developed the code SSB, also solving the forward master equations, which added the ability to model six groups of delayed neutron precursors. However, when extending to space and energy-dependent systems, the Pál-Bell equations must be solved (Williams and Eaton, 2017, 2018, 2020). Cooling et al. (2018) developed the CALLISTO-SPK code which efficiently solves the energy-dependent Pál-Bell equations. The relationship between the forward and backward (Pál-Bell) master equations and their respective advantages and disadvantages has been explained by Williams (2023).

The Pál-Bell equations, shown in Appendix A, are able to model the full fission multiplicity through the variable χ. However, a limitation of the Pál-Bell equations is the inability to accommodate changes in the macroscopic neutron cross-sections arising from temperature and void changes or other physical processes (Pázsit and Pál, 2007; Williams, 2023). This paper investigates the consequence of this limitation, in relation to low neutron source NPP start-up safety calculations, using an Itô-calculus approach. While in principle the forward form of the PDF is valid with feedback, the moment equations as devised by (Harris, 1958) suffer from the closure problem, namely that there are more equations than unknowns. To deal with this matter requires some assumptions about the PDF so that a higher moment can be expressed in terms of lower moments. We attempted this task but found that the associated numerical work too great a task and extensive for this paper. That is why the Itô method, which is not exact, but allows the effect of feedback to be included without too much effort is used.

Itô-calculus approaches are approximate methods that can be used to model neutron kinetics using the mean and standard deviation in the change in particle populations in time dt. While the Pál-Bell equations utilise the full fission multiplicity, Itô-calculus only uses the mean and standard deviation. However, previous publications have used Itô-calculus approaches to great effect in modelling the fast burst GODIVA experiments and replicating the results of the point kinetic equations.

Itô-calculus approaches may offer a good adjunct model for verification purposes, as they are derived using independent mathematical formalisms. Adjunct models may aid independent verification of nuclear reactor start-up operations which have very stringent controls in terms of probabilistic nuclear reactor safety analysis and assessment. Furthermore, such independent models could assist nuclear regulators, and technical safety organisations (TSOs), in assessing Modelling & Simulation (M&S) methods for low neutron source start-up simulations.

1.1. Modelling low neutron source NPP start-up physics

Multiple studies have explained the method for ensuring an NPP start-up procedure is sufficiently safe (Williams and Eaton, 2017, 2020; Cooling et al., 2018). A brief outline of the procedure will be presented here. For a given neutron source strength, S, and reactivity profile $\rho(t)$, the time at which the shape of the neutron population mean-normalised CDF stops changing must be computed. Good indicators of this time are when the neutron and delayed neutron precursor relative standard deviations, $\mathrm{RSD_n}$ and $\mathrm{RSD_p}$ respectively, converge (Williams and Eaton, 2017, 2020), or when $\mathrm{RSD_n}$ stops changing (Williams, 2020). These are known as the maturity time, t_{mat}, of the system. At t_{mat}, the stochastic source reduction factor (SSRF):

$$M = \frac{\bar{n}(t_{\mathrm{mat}})}{n^*} \tag{1}$$

must be found, viz:

$$Q(n^*, t_{\mathrm{mat}}) = \sum_{n=0}^{n^*-1} P(n, t_{\mathrm{mat}}) \tag{2}$$

where, $Q(n^*, t_{\mathrm{mat}})$ is the cumulative probability that there are fewer than n^* neutrons present in the system at t_{mat}, $\bar{n}(t_{\mathrm{mat}})$ is the mean neutron population at t_{mat}, and n^* is determined by the desired safety probability Q (usually 10^{-8}-10^{-5}).

For a desired safety probability Q, a reduced neutron source strength:

$$S_{\mathrm{m}} = S\frac{n^*}{\bar{n}(t_{\mathrm{mat}})} = \frac{S}{M}, \tag{3}$$

is then used in a deterministic nuclear reactor start-up simulation that incorporates thermal and reactivity feedback mechanisms to model the peak power, temperature, pressure, and reactivity achieved during the start-up operation. If these parameters do not exceed design limits, then the start-up procedure is determined to have a safety probability equal to Q. Typically, values of Q between 10^{-8}-10^{-5} are used (Williams and Eaton, 2017, 2020). Appendix A shows the mono-energetic point kinetic Pál-Bell equations used in this study and Appendix B details how the Pál-Bell equations are used to perform the analysis in Section 1.1. For further details regarding the methodology and explanation, see Hannauer (1963), Williams and Eaton (2017, 2020).

Thermal feedback mechanisms are not modelled when computing t_{mat} or $Q(n^*, t_{\mathrm{mat}})$ for multiple reasons. Firstly, it is assumed that the mean neutron population is small enough at t_{mat} that the effects of thermal feedback are negligible. Secondly, as mentioned previously, the Pál-Bell equations used to compute $Q(n^*, t_{\mathrm{mat}})$ are unable to accommodate changes in the macroscopic neutron cross-sections arising from feedback processes. Lastly, it is assumed that the shape of the neutron population CDF will remain constant after t_{mat} and thermal feedback starts to effect the system.

This paper uses an Itô-calculus approach to model NPP start-up and investigate the impact of neglecting thermal feedback within the Pál-Bell equations.

2. Computational method and approach

2.1. Discretisation scheme

In this study, we will use an Itô-calculus approach derived by Hayes and Allen (2005) to model the stochastic nuclear reactor kinetics during low neutron source NPP start-up. Various discretisation schemes have been used to model the Itô stochastic differential system of equations, for example, explicit Euler–Maruyama (Saha Ray and Patra, 2013), implicit Euler–Maruyama (Suescun-Diaz et al., 2018), diagonalisation decomposition method (da Silva et al., 2016), and analytical polynomial inversion (Hayes and Allen, 2005; Aboanber and Nahla, 2002).

Hayes and Allen (2005) show that the neutron and delayed neutron precursor population may be computed with the following discretisation scheme:

$$\vec{x}_{i+1} = X_i e^{D_i h_i} X_i^{-1} \left\{ \left[\vec{x}_i + h\vec{F}(t_i)\right] + \sqrt{h}\hat{B}^{\frac{1}{2}}\vec{\eta}_i \right\}, \tag{4}$$

where the time-step size is $h_i = t_{i+1} - t_i$, $\vec{x}_i$ is the array of neutron and M precursor group populations at time-step i:

$$\vec{x} = \begin{bmatrix} n \\ c_1 \\ c_2 \\ \vdots \\ c_M \end{bmatrix}, \tag{5}$$

where $\vec{F}(t)$ is the source array with neutron source strength $S(t)$:

$$\vec{F}(t) = \begin{bmatrix} S(t) \\ 0 \\ 0 \\ \vdots \\ 0 \end{bmatrix}, \tag{6}$$

and $\hat{B}$ is the matrix:

$$\hat{B} = \begin{bmatrix} \zeta & a_1 & a_2 & \cdots & a_M \\ a_1 & r_1 & b_{2,3} & \cdots & b_{2,M+1} \\ a_2 & b_{3,2} & r_2 & \ddots & \vdots \\ \vdots & \vdots & \ddots & \ddots & b_{M,M+1} \\ a_M & b_{M+1,2} & \cdots & b_{M+1,M} & r_M \end{bmatrix} \tag{7}$$

where

$$\zeta = \gamma n + \sum_{m=1}^{M} \lambda_m c_m + S \tag{8}$$

$$\gamma = \frac{-1 - \rho + 2\beta + (1-\beta)^2\overline{\nu}}{l} \tag{9}$$

$$a_m = \frac{\beta_m}{l}[-1 + (1-\beta)\overline{\nu}]n - \lambda_m c_m \tag{10}$$

$$b_{m,k} = \frac{\beta_{m-1}\beta_{k-1}\overline{\nu}}{l} n \tag{11}$$

and

$$r_m = \frac{\beta_m^2\overline{\nu}}{l} n + \lambda_m c_m. \tag{12}$$

The elements of vector $\vec{\eta}_i$ are normally distributed with mean zero and variance unity.

Lastly, $X_i D_i X_i^{-1} = \hat{A}_i$, where

$$\hat{A}_i = \begin{bmatrix} \frac{\rho(t_i)-\beta}{l} & \lambda_1 & \lambda_2 & \cdots & \lambda_M \\ \frac{\beta_1}{l} & -\lambda_1 & 0 & \cdots & 0 \\ \frac{\beta_2}{l} & 0 & -\lambda_2 & \ddots & \vdots \\ \vdots & \vdots & \ddots & \ddots & 0 \\ \frac{\beta_M}{l} & 0 & \cdots & 0 & -\lambda_M \end{bmatrix} \tag{13}$$

where the columns of X_i and the diagonal elements of D_i are the eigenvectors and eigenvalues of $\hat{A}_i$ respectively.

2.2. Thermal feedback model

In this study, we consider a simple temperature feedback model and corresponding Itô-calculus approximation (Nahla, 2017), viz:

$$\frac{dN}{dt} = \frac{\rho(t) - \beta}{\Lambda} N(t) + \sum_{i=1}^{M} \lambda_i C_i + S(t) \tag{14}$$

$$\frac{dC_i}{dt} = \frac{\beta_i}{\Lambda} N(t) - \lambda_i C_i(t) \qquad \text{for } i = 1, M \tag{15}$$

$$\rho(t) = \rho_{\text{ex}}(t) - \alpha\left[T(t) - T_0\right] \tag{16}$$

$$\frac{dT}{dt} = K_c N(t) \tag{17}$$

where $N(t)$ is the neutron population at time t, $\rho(t)$ is the total reactivity, $\rho_{\text{ex}}(t)$ is the external reactivity, $C_i(t)$ is the population of delayed neutron precursor group i, β_i delayed neutron fraction of group i, λ_i is the decay constant of group i, Λ is the neutron generation time, $T(t)$ is the temperature of the reactor at time t (with units K), T_0 is the initial temperature of the reactor, α is the temperature coefficient of reactivity (with units 1/K), and K_c is the reciprocal of the thermal capacity of the reactor (with units K/MWs).

Nahla (2017) showed that feedback caused by Newton's law of cooling can be incorporated into the Itô-calculus approach using the following approximation:

$$\rho(t_i) \approx \rho_{\text{ex}}(t_{i+1}) - h\xi \sum_{j=0}^{i} N(t_j) \tag{18}$$

where $h = t_{i+1} - t_i$ is the time-step, and $\xi = \alpha K_c$ (with units 1/MWs) is the feedback term. Inserting (18) into (9) and (13) results in an Itô-calculus model containing the temperature feedback mechanism (14)–(17).

2.3. Method for determining the effect of neglecting thermal feedback within the Pál-Bell equations

During NPP start-up, when neglecting thermal feedback, the shape of the mean-normalised neutron population CDF does not change after the maturity time. In other words, the shape of the neutron population distribution in relation to the mean neutron population stops changing. Therefore, only the mean neutron population is required after t_{mat} to generate the full distribution. Furthermore, in the absence of thermal feedback, the ratio of the mean neutron population between two systems is equal to the ratio of their respective neutron source strengths:

$$\frac{\bar{N}_1(t)}{\bar{N}_2(t)} = \frac{S_1}{S_2}. \tag{19}$$

Additionally, it is known that the deterministic peak neutron population during start-up is proportional to the ramp rate and inversely proportional to the neutron source strength.

Therefore, if the ratio $\bar{n}(t_{\text{mat}})/n^*$ is found for the cumulative probability Q, the system with neutron source strength S will produce neutron peak populations greater than the system with neutron source strength S_{m} with probability Q.

The method in Section 1.1 assumes that the shape of the mean-normalised CDF at the maturity time, found in the absence of thermal feedback, is the same as that of the distribution in the peak neutron populations when thermal feedback mechanisms are considered.

This paper investigates whether the safety probability calculated while ignoring thermal feedback produces safe start-up transients when thermal feedback is incorporated into the stochastic model. Furthermore, the consequence of thermal feedback considerably impacting the mean-normalised neutron population CDF before the maturity time is investigated.

The following procedures are employed to investigate the role of thermal feedback during NPP start-up:

Validation and Verification (V&V) of Implementation

1. Verify the mean and standard deviation calculated using the Itô-calculus approach against existing benchmark results in the literature. This analysis is shown in Appendix C.
2. Use the Itô-calculus approach to compute the wait-time probability distribution for various fast reactor start-up experiments and compare the results against the published experimental results.
3. Compare the neutron population CDF at the maturity time of various NPP start-up routines computed using the Itô-calculus approach and the Pál-Bell equations.
4. Compare the mean neutron population (modelling thermal feedback) computed using the Itô-calculus approach and the point kinetics equations.

Investigating the Effect of Thermal Feedback

1. Use the Itô-calculus approach to compute the neutron population CDF at the maturity time of various NPP start-up routines, given neutron source strength S while neglecting thermal feedback.
2. Use the Itô-calculus approach to compute the deterministic peak neutron population during the NPP start-up routines (while modelling thermal feedback), given neutron source strengths S_{m}, calculated at various Q values and while neglecting thermal feedback.
3. Use the Itô-calculus approach to compute the distribution in the peak neutron population during the NPP start-up routines (while modelling thermal feedback), given neutron source strength S.
4. Compare the probability of safe start-ups using thermal feedback against the probabilities calculated neglecting thermal feedback.

2.4. Algorithms

The algorithms used to compute the neutron population moments (mean and standard deviation), the neutron population CDF, the SSRF, and the wait-time probability distribution are shown below.

Algorithm 1 An algorithm to compute the neutron and delayed neutron precursor population mean $\bar{X}$ and standard deviation σ_X up to a desired time t_{end} using a prescribed number of realisations r. The columns $\bar{X}[:,i]$ and $\sigma_X[:,i]$ are the mean and standard deviation of the population array at time t_i.

$\bar{X} \leftarrow 0$
$\sigma_X \leftarrow 0$
$j \leftarrow 0$
for $j \leq r$ **do**
  $j \leftarrow j+1$
  $t \leftarrow 0$
  $i \leftarrow 0$
  $\vec{x} \leftarrow [N_0, \frac{N_0\beta_1}{\lambda_1\Lambda}, \frac{N_0\beta_2}{\lambda_2\Lambda}, \cdots, \frac{N_0\beta_6}{\lambda_6\Lambda}]$
  while $t \leq t_{\mathrm{end}}$ **do**
    $t \leftarrow t+h$
    $\vec{x} \leftarrow$ (4)
    $\bar{X}[:,i+1] \leftarrow \vec{x}$
    $\sigma_X[:,i+1] \leftarrow (\vec{x})^2$
    $i \leftarrow i+1$
$\bar{X} \leftarrow \frac{\bar{X}}{r}$
$\sigma_X \leftarrow \sqrt{\frac{\sigma_X}{r} - \bar{X}^2}$

3. Results

3.1. Validating against caliban fast burst reactor wait-time cumulative distribution functions (CDFs)

Firstly, the Itô-calculus implementation in this study is used to compute the wait-time cumulative distribution function (CDF) of three delayed super-critical Caliban fast burst reactor start-up experiments. Authier et al. (2014) published experimental data on the initiation of persistent fission chains, at different delayed super-critical states, using the fast burst nuclear reactor Caliban. The time for Caliban to build up to 2×10^9 fissions/s following a start-up routine was measured multiple times for three different final reactivities ($\rho = 0.206 \pm 0.002$\$, $\rho = 0.255 \pm 0.001$\$, and $\rho = 0.272 \pm 0.001$\$).

One method for modelling the wait-time CDF for prompt super-critical experiments is to compute the survival probability (Humbert and Méchitoua, 2004). However, this method is not applicable to delayed super-critical experiments. Previously, Williams has shown that the Gamma probability distribution function can be used to effectively model these delayed super-critical wait-time experiments (Williams, 2017).

In this paper, each start-up experiment is simulated with 500 Itô-calculus realisations with a time-step $h = 0.1$ s. The initial conditions are: $\vec{x}_0 = [N_0, \frac{N_0\beta_1}{\lambda_1\Lambda}, \frac{N_0\beta_2}{\lambda_2\Lambda} \cdots]$ where $N_0 = \frac{S\Lambda}{-\rho(t=0)}$. Each realisation was computed until the fission rate exceeded 2×10^9 fissions/s; the

Algorithm 2 An algorithm to compute the wait-time probability distribution function $\vec{p}_{\mathrm{w}}$, for a neutron threshold $n_{\mathrm{threshold}}$ using a prescribed number of realisations r.

$\vec{p}_{\mathrm{w}} \leftarrow 0$
$j \leftarrow 0$
for $j \leq r$ **do**
  $j \leftarrow j+1$
  $t \leftarrow 0$
  $\vec{x} \leftarrow [N_0, \frac{N_0\beta_1}{\lambda_1\Lambda}, \frac{N_0\beta_2}{\lambda_2\Lambda}, \cdots, \frac{N_0\beta_6}{\lambda_6\Lambda}]$
  while $\vec{x}(0) < n_{\mathrm{threshold}}$ **do**
    $t \leftarrow t+h$
    $\vec{x} \leftarrow$ (4)
  $\vec{p}_{\mathrm{w}}(j) \leftarrow t$
$\vec{p}_{\mathrm{w}} \leftarrow sort(\vec{p}_{\mathrm{w}})$
Plot $\vec{p}_{\mathrm{w}}$ against $[\frac{1}{r}, \frac{2}{r}, \cdots, \frac{r}{r}]$

Algorithm 3 An algorithm to compute the neutron population CDF at the maturity time t_{mat}, using a prescribed number of realisations r.

$\vec{n}^* \leftarrow 0$
$j \leftarrow 0$
for $j \leq r$ **do**
  $j \leftarrow j+1$
  $t \leftarrow 0$
  $\vec{x} \leftarrow [N_0, \frac{N_0\beta_1}{\lambda_1\Lambda}, \frac{N_0\beta_2}{\lambda_2\Lambda}, \cdots, \frac{N_0\beta_6}{\lambda_6\Lambda}]$
  while $t < t_{\mathrm{mat}}$ **do**
    $t \leftarrow t+h$
    $\vec{x} \leftarrow$ (4)
  $\vec{n}^*(j) \leftarrow \vec{x}(0)$
$\vec{n}^* \leftarrow sort(\vec{n}^*)$
$\vec{q} \leftarrow [\frac{1}{r}, \frac{2}{r}, \cdots, \frac{r}{r}]$
Plot $\vec{n}^*$ against $\vec{q}$

Algorithm 4 An algorithm to compute the SSRF, for a desired safety probability Q, given the neutron population CDF at the maturity time and using a prescribed number of realisations r.

$\vec{q} \leftarrow [\frac{1}{r}, \frac{2}{r}, \cdots, \frac{r}{r}]$
$\vec{n}^* \leftarrow sort(\vec{n}^*)$
$\bar{N} \leftarrow \frac{1}{r}\sum_{j=1}^{r} \vec{n}^*(j)$
$\vec{M} \leftarrow \frac{\bar{N}}{\vec{n}^*}$
$i \leftarrow 0$
while $\vec{q}(i) < Q$ **do**
  $i \leftarrow i+1$
SSRF $\leftarrow \frac{Q-\vec{q}(i-1)}{\vec{q}(i)-\vec{q}(i-1)}\left[\vec{M}(i) - \vec{M}(i-1)\right] + \vec{M}(i-1)$

Table 1
The group data (Humbert and Méchitoua, 2004) and multiplicity data (Pázsit and Pál, 2007) used for the Caliban simulation with the neutron source strength $S = 200\,\mathrm{n/s}$ and the generation time $\Lambda = 12 \times 10^{-9}$ s (Authier et al., 2014).

Group/Multiplicity	p_{fn}	$\frac{1}{\lambda_i}(s)$	$\beta_i(\times 10^{-5})$
0	0.0317	–	–
1	0.1720	80.645	21.73
2	0.3363	32.785	143.79
3	0.3038	9.009	130.34
4	0.1268	3.322	260.69
5	0.0266	0.885	76.55
6	0.0026	0.333	26.90
7	0.0002	–	–

Table 2
Reactivity profile for the Caliban fast burst experiments with final step reactivity $\rho_{\max}$ (Authier et al., 2014).

Time (s)	ρ($)	Time (s)	ρ($)	Time (s)	ρ($)	Time (s)	ρ($)
0.00	−16.829	55.00	−1.919	58.00	−0.063	61.08	0.143
16.67	−15.127	55.83	−1.403	58.08	−0.011	62.08	0.195
33.33	−11.572	56.67	−0.888	58.58	0.011	73.67	0.195
50.00	−5.012	57.50	−0.372	59.08	0.040	73.92	$\rho_{\max}$
54.17	−2.434	57.92	−0.114	60.08	0.092		

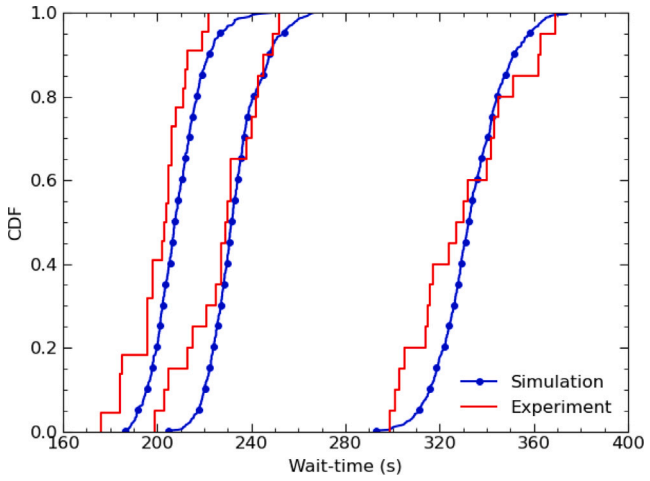

Fig. 1. A comparison of the wait-time CDF, for the fission rate to exceed 2×10^9 fissions/s, calculated using the Itô-calculus approach and three delayed super-critical Caliban fast burst nuclear reactor wait-time experiments (Authier et al., 2014). The results of the 0.206 $, 0.255 $, and 0.272 $ cases are shown from right to left.

elapsed times between the reactivity reaching $\rho_{\max}$ and the end of the simulations were recorded. These simulations do not include thermal feedback and simply validate the implementation of (4)–(13). The neutronic data used to model the Caliban fast burst nuclear reactor experiment are shown in Table 1. The reactivity profile used in the experiments is described by Authier et al. (2014) but is reproduced in Table 2 for clarity.

Fig. 1 compares the wait-time cumulative probability distribution, for the fission rate to exceed 2×10^9 fissions/s, of the three delayed super-critical experimental results against the Itô-calculus simulations. Table 3 quantitatively compares the experimental and simulated mean wait-time and the associated standard deviations. The results show good agreement and provide confidence in the implementation of (4)–(13).

3.2. Verification of the neutron population CDF against the Pál-Bell equations

Next, the mean-normalised neutron population CDF at the maturity time of various NPP start-up operations is computed using the Itô-calculus approach and compared against the CDF computed using the Pál-Bell equations. Two reactivity profiles are modelled, where Profile 1:

$$\rho(t) = \begin{cases} -1\,\$ + 0.01t\ \$/s, & \text{if } 0 \le t \le 200\,\mathrm{s}, \\ 1\,\$, & \text{otherwise}, \end{cases} \tag{20}$$

and Profile 2:

$$\rho(t) = \begin{cases} -1\,\$ + 0.001t\ \$/s, & \text{if } 0 \le t \le 2000\,\mathrm{s}, \\ 1\,\$, & \text{otherwise}. \end{cases} \tag{21}$$

Each NPP start-up profile is simulated with the neutron source strengths 1000 n/s and 2000 n/s. The initial conditions are: $\vec{x}_0 = [N_0, \frac{N_0\beta_1}{\lambda_1\Lambda}, \frac{N_0\beta_2}{\lambda_2\Lambda} \cdots]$ where $N_0 = \frac{S\Lambda}{-\rho(t=0)}$. The neutronic data used to model the systems in Section 3.2 are shown in Table 4.

The maturity times for Profiles 1 and 2, which are independent of neutron source strength (Williams and Eaton, 2017, 2020), have been calculated using the Pál-Bell equations, as 173.3 s, 1370.6 s respectively.

Each Itô-calculus simulation has been computed up to the maturity time of the respective NPP start-up profile. The neutron population at the end of each simulation has then been recorded. Variable time-step sizes have been used to compute each Itô-calculus realisation; the sub-critical regimes have been modelled with $h = 2.0$ s and $h = 20.0$ s for Profiles 1 and 2, respectively, while both profiles have used $h = 0.1$ s for the super-critical regimes. The larger time steps help reduce the computation times, while the smaller time steps facilitate greater refinement in the solution at the end of the simulation.

The CDFs computed using the Itô-calculus approach and Pál-Bell equations are compared for the range $10^{-5} < Q < 1$. Comparing this range requires a minimum of 10^5 Itô-calculus realisations for each NPP start-up routine. However, the solution at $Q = 10^{-5}$ will not have converged as only a single data point will exist at this probability. Therefore, we have simulated 10^6 Itô-calculus realisations.

Figs. 2(a)–2(b) show the mean-normalised neutron population CDF ($n^*/\bar{n}(t_{\mathrm{mat}})$ against Q) for Profiles 1 and 2 with neutron source strengths 1000 n/s and 2000 n/s. The Itô-calculus results have been computed using 10^6 realisations. However, at the Q values 10^{-5}, 10^{-4}, 10^{-3}, 10^{-2}, and 10^{-1}, the figures show the values $\left(n^*/\bar{n}(t_{\mathrm{mat}})\right)_i^Q$ which are the $n^*/\bar{n}(t_{\mathrm{mat}})$ values calculated with the ith 10^5 sample. Table 5 quantifies the relative difference (%) between the SSRF values computed using the Pál-Bell equations and the Itô-calculus approach.

The results show that the approximate adjunct Itô-calculus approach is able to compute SSRFs within ≤10% of the Pál-Bell results. While this level of agreement is inadequate for the Itô-calculus approach to

Table 3
A comparison of the mean wait-time $\langle t \rangle$ and associated standard deviation σ for the experimental Caliban results and simulated Itô-calculus results in Fig. 1.

Reactivity ($)	Experiment		Simulation	
	$\langle t \rangle(s)$	$\sigma(s)$	$\langle t \rangle(s)$	$\sigma(s)$
0.206	332.3	23.1	333.2	14.0
0.255	229.4	15.5	232.9	10.8
0.272	202.5	12.4	208.5	10.5

Table 4
The group and multiplicity data used for the NPP start-up simulation in Section 3.2. The generation time is $\Lambda = 12 \times 10^{-9}$ s.

Group/Multiplicity	p_{fn}	$\lambda_i(1/s)$	β_i
0	0.0317	–	–
1	0.1720	0.0125	0.0002
2	0.3363	0.0303	0.0013
3	0.3038	0.0955	0.0010
4	0.1268	0.2844	0.0030
5	0.0266	0.9782	0.0012
6	0.0026	3.4888	0.0006
7	0.0002	–	–

Table 5
The relative difference (%) between the values of $n^*/\bar{n}$ calculated by the Pál-Bell method and Itô-calculus approach for various values of Q.

$Q \setminus S$	$\dot{\rho}(t) = 0.01\$/s$		$\dot{\rho}(t) = 0.001\$/s$	
	1000 n/s	2000 n/s	1000 n/s	2000 n/s
10^{-5}	7.7	6.8	2.7	4.0
10^{-4}	8.0	7.2	4.5	3.9
10^{-3}	7.9	5.9	4.7	3.3
10^{-2}	6.0	4.0	3.3	2.3
10^{-1}	2.6	1.7	1.3	0.8

Table 6
The peak of the mean neutron population and time at which the peak occurs for various NPP start-up simulations.

S	ξ	$\hat{n}_{\text{PK}}$	$\langle \hat{n}_{\text{Itô}} \rangle$	$t(\hat{n}_{\text{PK}})$	$t(\langle \hat{n}_{\text{Itô}} \rangle)$
10	10^{-13}	2.02×10^{12}	2.06×10^{12}	1.38	1.38
	10^{-11}	1.54×10^{10}	1.57×10^{10}	1.30	1.30
	10^{-9}	1.05×10^{8}	1.07×10^{8}	1.21	1.21
100	10^{-13}	2.02×10^{12}	2.02×10^{12}	1.38	1.38
	10^{-11}	1.54×10^{10}	1.57×10^{10}	1.30	1.30
	10^{-9}	1.05×10^{8}	1.07×10^{8}	1.21	1.21
1000	10^{-13}	2.00×10^{12}	2.00×10^{12}	1.38	1.38
	10^{-11}	1.53×10^{10}	1.57×10^{10}	1.30	1.30
	10^{-9}	1.03×10^{8}	1.06×10^{8}	1.21	1.21

replace the Pál-Bell equations, the results demonstrate that the Itô-calculus approach can be used to gain useful insight into the behaviour of stochastic nuclear kinetics and dynamics during low neutron source NPP start-up.

However, it should be noted that the SSRFs $(\bar{n}(t_{\text{mat}})/n^*)$ calculated with the Itô-calculus approach are not conservative and therefore should not be used for safety-critical applications. Figs. 2(a)–2(b) show that as Q decreases, the spread of values $\left(n^*/\bar{n}(t_{\text{mat}})\right)_i^Q$ increases. The greater spread in the results is due to $1/Q$ approaching the number of realisations used to produce the distribution. The range of $\left(n^*/\bar{n}(t_{\text{mat}})\right)_i^Q$ values indicate the range of potential solutions if only 10^5 realisations were used. To improve the results at smaller values of Q, more realisations are required. However, increasing the number of realisations is computationally demanding.

3.3. Verification of the thermal feedback implementation

Next, the implementation of (18) is verified against the point kinetics Eqs. (14)–(17). The reactivity profile is $\rho_{\text{ext}}(t) = 0.01t$ with the thermal feedback parameters $\xi = 10^{-13}$, $\xi = 10^{-11}$, and $\xi = 10^{-9}$. The neutronic parameters are shown in Table 4. Three neutron source strengths are modelled: 10 n/s, 100 n/s, and 1000 n/s. The initial conditions are: $\vec{x}_0 = [N_0, \frac{N_0\beta_1}{\lambda_1\Lambda}, \frac{N_0\beta_2}{\lambda_2\Lambda} \cdots]$ where $N_0 = 100$. Each NPP start-up has been modelled with 1000 Itô-calculus realisations as only the mean neutron population is of interest when comparing against the point kinetics equations. Figs. 3–5 show the mean neutron population calculated using the point kinetics equations and two individual Itô-calculus realisations for the various NPP start-up routines. The mean ensemble of Itô-calculus realisations closely matches the point kinetics results and is undisguisable when plotted. Therefore, Table 6 shows the peak neutron populations calculated using both Itô-calculus and the point kinetics equations. The results show good agreement and suggest the correct implementation of (18).

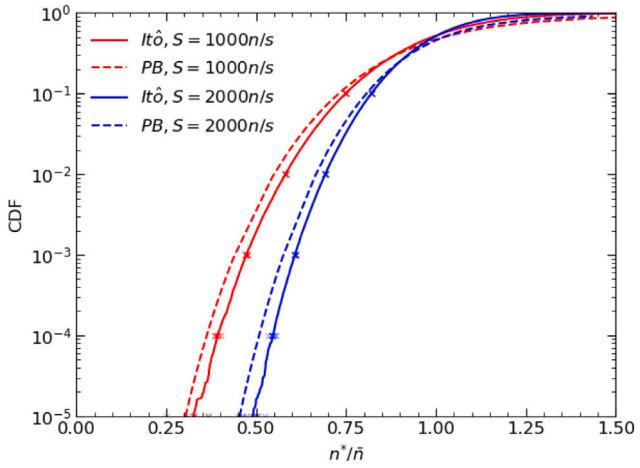

(a) The ramp rate is $\dot{\rho}(t) = 0.01\$/s$.

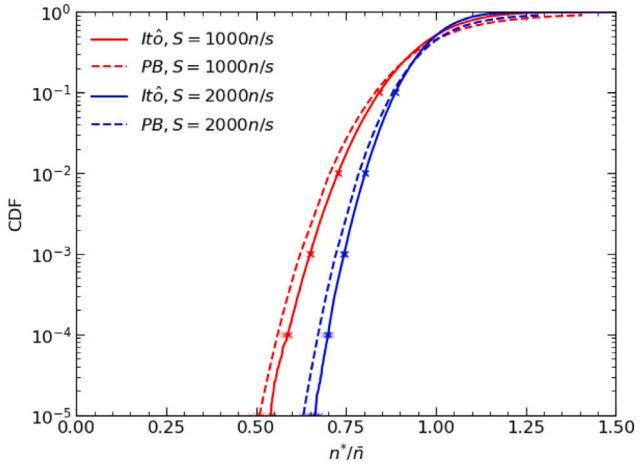

(b) The ramp rate is $\dot{\rho}(t) = 0.001\$/s$.

Fig. 2. A comparison of the mean-normalised neutron population CDF at t_{mat} calculated using the Itô-calculus approach (Itô) (solid lines) and the Pál-Bell equations (PB) (dashed lines). 10^6 Itô-calculus realisations were computed up to $t = t_{\text{mat}}$ and the final neutron populations were recorded. The solid lines show the results using 10^6 realisations. At each CDF value 10^{-5}, 10^{-4}, 10^{-3}, 10^{-2}, and 10^{-1}, ten scatter points are shown for each Itô curve; these scatter points show the value of $\left(n^*/\bar{n}\right)_i^Q$ using a sample 10^5 where $\left(n^*/\bar{n}\right)_{i=1}^{q=10^{-5}}$ represents the value of $n^*/\bar{n}$ at the CDF value 10^{-5} using the first 10^5 Itô-calculus realisations.

3.4. Investigating the impact of thermal feedback on low neutron source NPP start-up

The Itô-calculus approach is now used to calculate the distribution in peak neutron populations for the NPP start-up routines in Section 3.2. However, the Itô-calculus simulations now model thermal feedback with $\xi = 10^{-13}$ and $\xi = 10^{-11}$.

Firstly, the effect of thermal feedback on the mean neutron population at the maturity time is found. Figs. 6(a)–6(b) show the mean neutron population calculated using the Pál-Bell equations and a sample Itô-calculus realisation with $\xi = 10^{-13}$. The figures show that thermal feedback only starts to reduce the sample realisation after t_{mat}. However, the neutron transient is significantly affected by thermal feedback before t_{mat} for $\xi = 10^{-11}$, as shown in Figs. 7(a)–7(b).

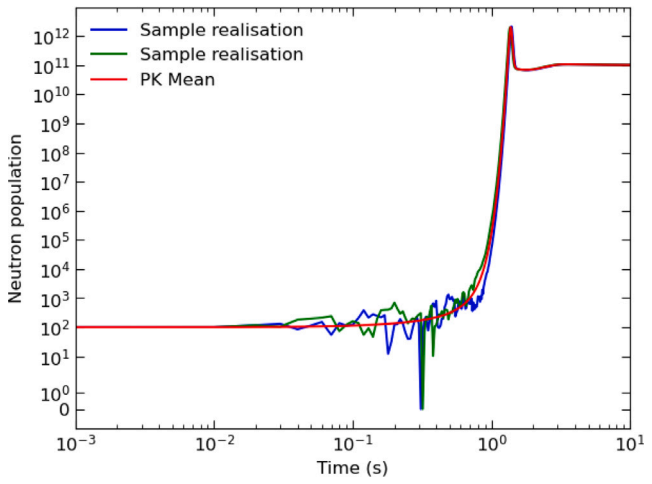

Fig. 3. Mean neutron population and two individual neutron sample paths for $S = 10\,\mathrm{n/s}$ and $\xi = 10^{-13}$.

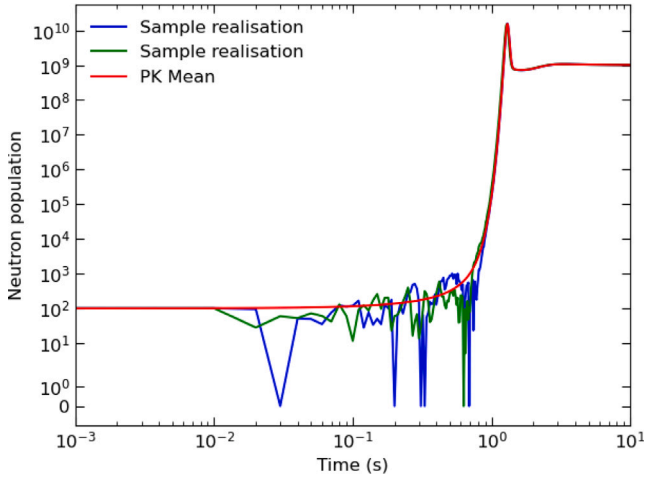

Fig. 4. Mean neutron population and two individual neutron sample paths for $S = 100\,\mathrm{n/s}$ and $\xi = 10^{-11}$.

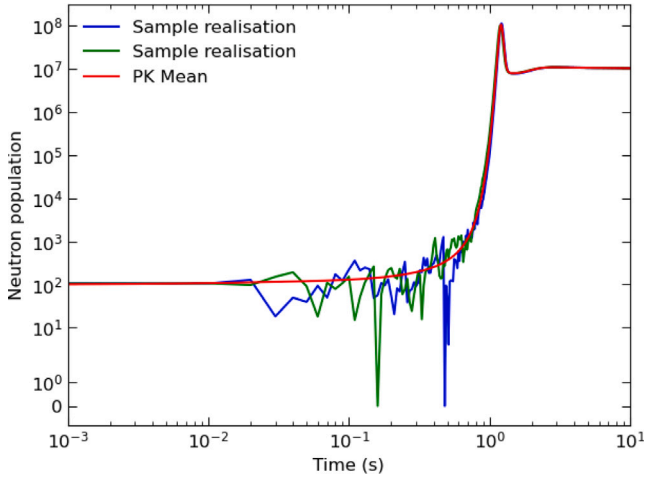

Fig. 5. Mean neutron population and two individual neutron sample paths for $S = 1000\,\mathrm{n/s}$ and $\xi = 10^{-9}$.

Next, the ten values of $\left(\frac{n^*}{\bar{n}(t_{\mathrm{mat}})}\right)_i^Q$ at each of the CDF values 10^{-5}, 10^{-4}, 10^{-3}, 10^{-2}, and 10^{-1} from Figs. 2(a)–2(b) (scatter points) have been used to calculate reduced neutron source strengths, S_{i}^Q. These values of S_{i}^Q have been calculated neglecting thermal feedback. Each of these reduced neutron source strengths S_{i}^Q has then been used in 100 Itô-calculus realisations which include thermal feedback. These realisations have been simulated until the neutron population has peaked due to the effect of thermal feedback. The peak neutron populations have been averaged over the 100 realisations, $\langle \hat{n} \rangle_i^Q$, and recorded as the expected peak for the neutron source strength S_{i}^Q. The range of values $\langle \hat{n} \rangle_i^Q$ for $i = 1, 2, \ldots, 10$ are displayed for each value of Q in Figs. 8–15 as error bars (black lines with an X at the mean). These error bars indicate the ideal distribution in the peak neutron population when the original neutron source strength is simulated, given thermal feedback has not influenced the neutron population distribution.

Subsequently, the original neutron source strengths (1000 n/s and 2000 n/s) have been used to model the NPP start-up routines with the given thermal feedback parameters $\xi = 10^{-11}$ and $\xi = 10^{-13}$. 10^5 Itô-calculus realisations have been simulated until the neutron population starts to decrease due to thermal feedback. The peak neutron population of each simulation has been recorded and the distributions are shown in Figs. 8–15. These results are tabulated in Table 7.

The results show excellent agreement between the peak neutron population distributions including thermal feedback, using the original neutron source strengths and using the reduced neutron source strength calculated with SSRFs neglecting thermal feedback.

Furthermore, the agreement between the peak neutron distributions for Figs. 8, 10, 12, and 14 show that SSRFs can be calculated neglecting thermal feedback, like the Pál-Bell equations, even if thermal feedback would significantly affect the mean neutron population before the maturity time.

4. Conclusions

In this paper, we have validated an Itô-calculus approach to modelling stochastic nuclear reactor kinetics against three delayed supercritical Caliban fast burst nuclear reactor experiments. Overall, the results showed good agreement between the numerical models and the experiments.

Furthermore, the Itô-calculus approach was used to model low neutron source NPP start-up calculations. The mean-normalised neutron population CDF at the maturity time was generated by simulating 10^6 Itô-calculus realisations for multiple NPP start-ups. The results showed adequate agreement with the results computed using the Pál-Bell equations. However, the SSRFs calculated using the Itô-calculus approach were not conservative. Therefore, the Itô-calculus approach can offer good insight into the behaviour and distribution of the scalar neutron flux during low neutron source NPP start-up. However, it is not recommended to use this approach for safety-critical applications. This is due to the stringent numerical accuracy requirements needed when computing safety probabilities for stochastic power surges that might damage the nuclear fuel.

In addition, the SSRFs for various safety probabilities were computed while ignoring thermal feedback. These SSRFs were used to compute the peak neutron population achieved, for neutron source strengths $S/SSRF$, during NPP start-up operations that modelled thermal feedback. These peak neutron populations were then compared against the distribution in peak neutron populations achieved using the original neutron source strengths. Excellent agreement was found between the results. These results indicate that the absence of thermal feedback in the Pál-Bell equations does not impact the final safety probability given the maturity time occurs before the mean neutron population is influenced by thermal feedback. This is a highly significant result from a nuclear reactor safety perspective and the first time this has been demonstrated conclusively in the research literature.

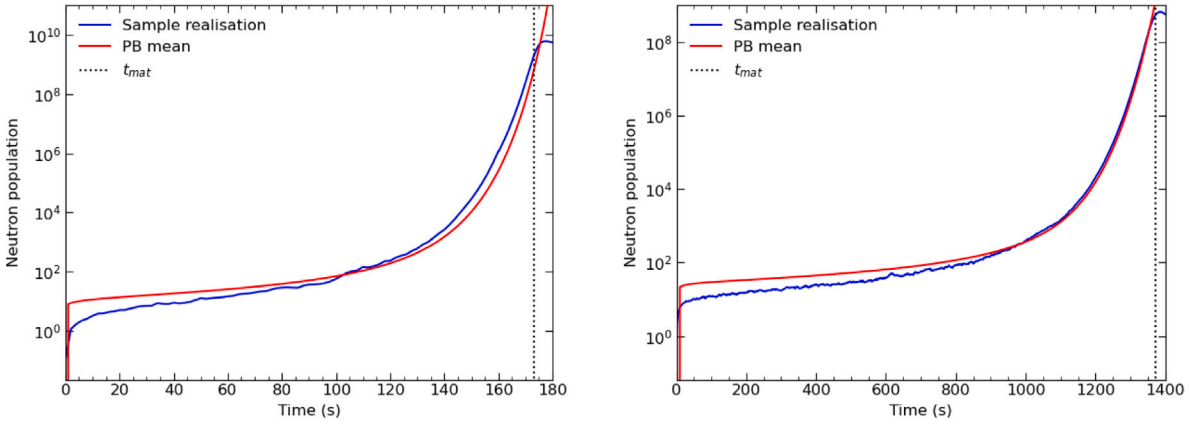

(a) The ramp rate is $\dot{\rho}(t) = 0.01\$/s$. The neutron source strength is 1000 n/s.

(b) The ramp rate is $\dot{\rho}(t) = 0.001\$/s$. The neutron source strength is 2000 n/s.

Fig. 6. The mean neutron population calculated by the Pál-Bell equations (PB) without thermal feedback and a sample Itô-calculus realisation which includes thermal feedback with $\xi = 10^{-13}$.

Table 7
The distribution in the peak neutron population $\hat{n}_Q$ that occurs with a cumulative probability Q, given a ramp rate $\dot{\rho}$, neutron source strength S, thermal feedback parameter ξ. The results are compared against the range in peak neutron populations calculated using the ten neutron source strengths $S_{m,i} = S/M_i$, where M_i is the stochastic source reduction factor calculated using 100,000 Itô-calculus realisations.

$\dot{\rho}$	S	ξ	$\hat{n}_{Q=10^{-5}}$	Range	$\hat{n}_{Q=10^{-3}}$	Range	$\hat{n}_{Q=10^{-1}}$	Range
0.01	1000	10^{-13}	6.79×10^9	$6.76–6.88\times10^9$	6.68×10^9	$6.67–6.68\times10^9$	6.53×10^9	$6.52–6.53\times10^9$
		10^{-11}	5.34×10^7	$5.24–5.35\times10^7$	5.15×10^7	$5.06–5.07\times10^7$	4.98×10^7	$4.98–4.99\times10^7$
	2000	10^{-13}	6.45×10^9	$6.43–6.47\times10^9$	6.38×10^9	$6.37–6.39\times10^9$	6.28×10^9	$6.27–6.28\times10^9$
		10^{-11}	4.91×10^7	$4.87–4.92\times10^7$	4.80×10^7	$4.79–4.80\times10^7$	4.70×10^7	$4.69–4.70\times10^7$
0.001	1000	10^{-13}	6.51×10^8	$6.46–6.58\times10^8$	6.33×10^8	$6.33–6.35\times10^8$	6.09×10^8	$6.08–6.09\times10^8$
		10^{-11}	4.30×10^6	$4.28–4.36\times10^6$	4.11×10^6	$4.10–4.12\times10^6$	3.89×10^6	$3.89–3.91\times10^6$
	2000	10^{-13}	6.66×10^8	$6.62–6.67\times10^8$	6.58×10^8	$6.58 – 6.59 \times 10^8$	6.50×10^8	$6.49–6.50\times10^8$
		10^{-11}	4.28×10^6	$4.26–4.31\times10^6$	4.20×10^6	$4.19–4.20\times10^6$	4.10×10^6	$4.09–4.10\times10^6$

CRediT authorship contribution statement

T.L. Gordon: Conceptualization, Data curation, Formal analysis, Investigation, Methodology, Software, Visualization, Writing – original draft, Writing – review & editing. **M.M.R. Williams:** Conceptualization, Methodology, Writing – review & editing. **M.D. Eaton:** Conceptualization, Funding acquisition, Methodology, Writing – review & editing. **P. Haigh:** Funding acquisition, Writing – review & editing.

Declaration of competing interest

The authors declare that they have no known competing financial interests or personal relationships that could have appeared to influence the work reported in this paper.

Data availability

In accordance with EPSRC funding requirements all supporting data used to create figures in this paper may be accessed at the following URL: https://zenodo.org/records/10776943.

Acknowledgements

Mr T.L. Gordon would like to acknowledge the support of Engineering and Physical Sciences Research Council (EPSRC) through the Doctoral Training Partnership (DTP) PhD scheme (EPSRC Grant number: EP/R513052/1). Mr T.L. Gordon and Dr M.D. Eaton would also like to acknowledge the financial support of Rolls-Royce, UK.

Appendix A. The mono-energetic point kinetic Pál-Bell equations

The spatially-independent, mono-energetic Pál Bell equations are presented here for clarity regarding the equations and methods used in this study. For a full mathematical derivation of the equations, see Pál (1961a,b,c). Assuming only one neutron emission per extraneous neutron source disintegration, the Pál-Bell equations may be written as (Pázsit and Pál, 2007):

$$-\frac{1}{v}\frac{\partial \tilde{G}(z,t|s)}{\partial s} = -\Sigma_{\mathrm{a}}(s)\tilde{G} + \Sigma_{\mathrm{f}}(s) - \Sigma_{\mathrm{f}}(s)H(\tilde{G},\tilde{G}_{\mathrm{d}m}), \tag{A.1}$$

$$-\frac{\partial \tilde{G}_{\mathrm{d}m}(z,t|s)}{\partial s} = \lambda_m(\tilde{G} - \tilde{G}_{\mathrm{d}m}), \tag{A.2}$$

$$\frac{\partial G_{\mathrm{s}}(z,t|s)}{\partial s} = S(s)G_{\mathrm{s}}\tilde{G}^n, \tag{A.3}$$

with

$$H(\tilde{G},\tilde{G}_{\mathrm{d}m}) = \sum_{n=0}^{\nu_{\max}} \frac{(-1)^n}{n!}\chi_n\tilde{G}^n \prod_{m=1}^{M}(1-\bar{\nu}\beta_m\tilde{G}_{\mathrm{d}m}), \tag{A.4}$$

and the final conditions

$$\tilde{G}(z,t|t) = 1 - z, \tag{A.5}$$

$$\tilde{G}_{\mathrm{d}m}(z,t|t) = 0, \tag{A.6}$$

$$G_{\mathrm{S}}(z,t|t) = 1. \tag{A.7}$$

where Σ_{a} is the macroscopic absorption cross-section, Σ_{f} is the macroscopic fission cross-section, λ_m is the delayed neutron precursor decay constant of group m, β_m is the delayed neutron precursor fraction of group m, S is the neutron source strength, χ is the fission multiplicity,

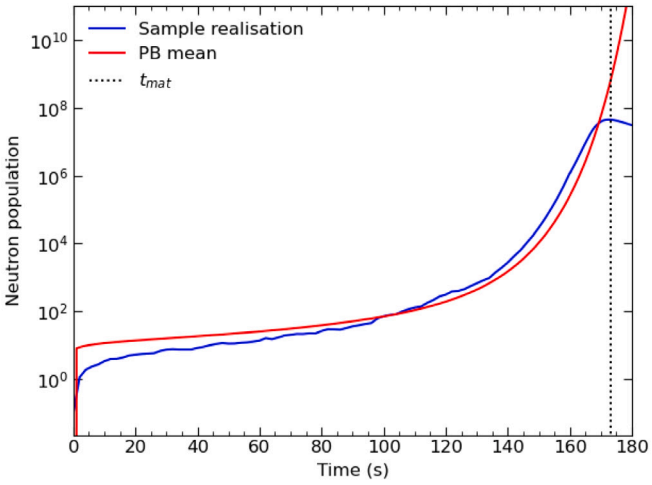

(a) The ramp rate is $\dot{\rho}(t) = 0.01\$/s$. The neutron source strength is 1000 n/s.

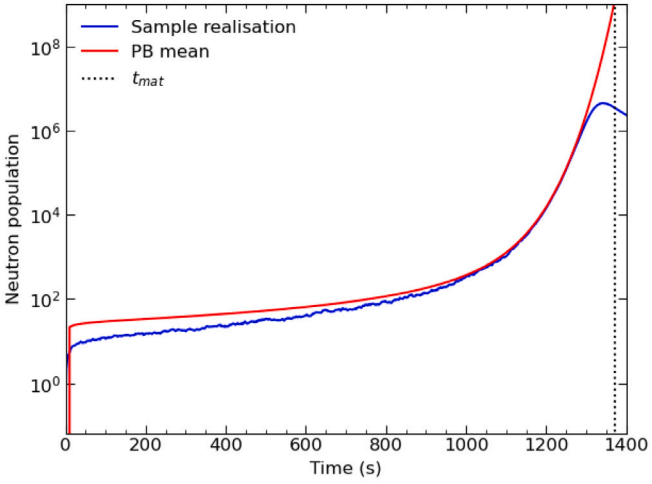

(b) The ramp rate is $\dot{\rho}(t) = 0.001\$/s$. The neutron source strength is 2000 n/s.

Fig. 7. The mean neutron population calculated by the Pál-Bell equations (PB) without thermal feedback and a sample Itô-calculus realisation which includes thermal feedback with $\xi = 10^{-11}$.

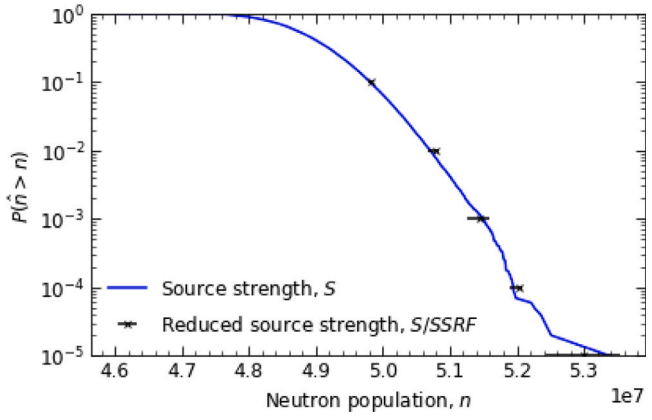

Fig. 8. The distribution in the peak neutron population for 100,000 Itô-calculus realisations for profile 1 and $\xi = 1 \times 10^{-11}$. The distribution is compared against the mean peak neutron populations calculated using the reduced source strengths $S/SSRF$ for the SSRFs at Q equal to 10^{-5}, 10^{-4}, 10^{-3}, 10^{-2}, and 10^{-1}.

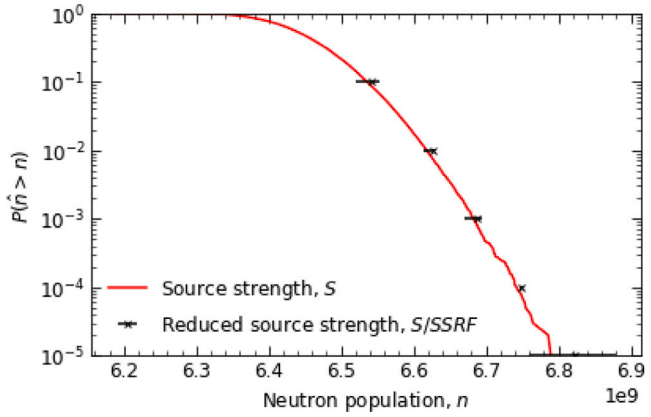

Fig. 9. The distribution in the peak neutron population for 100,000 Itô-calculus realisations for profile 1 and $\xi = 1 \times 10^{-13}$. The distribution is compared against the mean peak neutron populations calculated using the reduced source strengths $S/SSRF$ for the SSRFs at Q equal to 10^{-5}, 10^{-4}, 10^{-3}, 10^{-2}, and 10^{-1}.

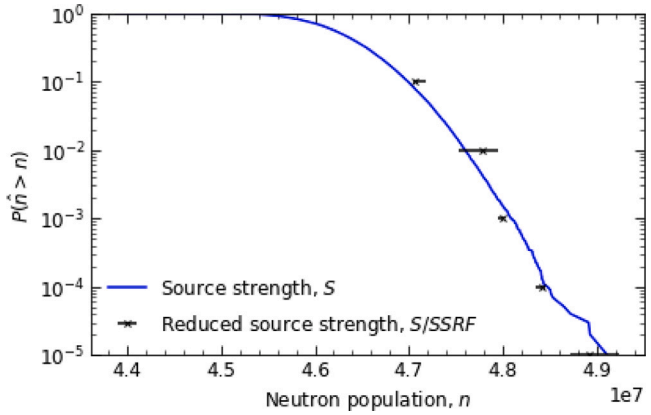

Fig. 10. The distribution in the peak neutron population for 100,000 Itô-calculus realisations for profile 2 and $\xi = 1 \times 10^{-11}$. The distribution is compared against the mean peak neutron populations calculated using the reduced source strengths $S/SSRF$ for the SSRFs at Q equal to 10^{-5}, 10^{-4}, 10^{-3}, 10^{-2}, and 10^{-1}.

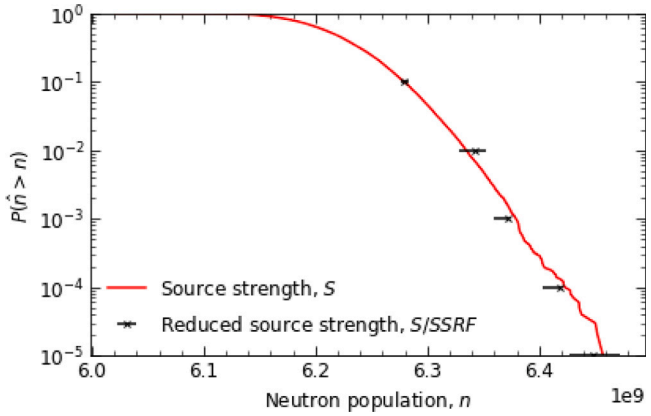

Fig. 11. The distribution in the peak neutron population for 100,000 Itô-calculus realisations for profile 2 and $\xi = 1 \times 10^{-13}$. The distribution is compared against the mean peak neutron populations calculated using the reduced source strengths $S/SSRF$ for the SSRFs at Q equal to 10^{-5}, 10^{-4}, 10^{-3}, 10^{-2}, and 10^{-1}.

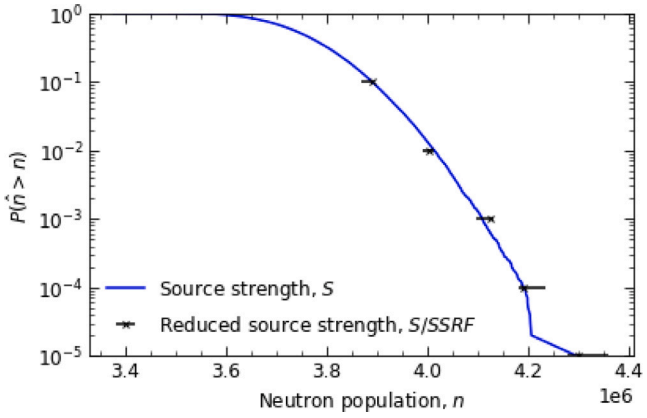

Fig. 12. The distribution in the peak neutron population for 100,000 Itô-calculus realisations for profile 3 and $\xi = 1 \times 10^{-11}$. The distribution is compared against the mean peak neutron populations calculated using the reduced source strengths $S/SSRF$ for the SSRFs at Q equal to 10^{-5}, 10^{-4}, 10^{-3}, 10^{-2}, and 10^{-1}.

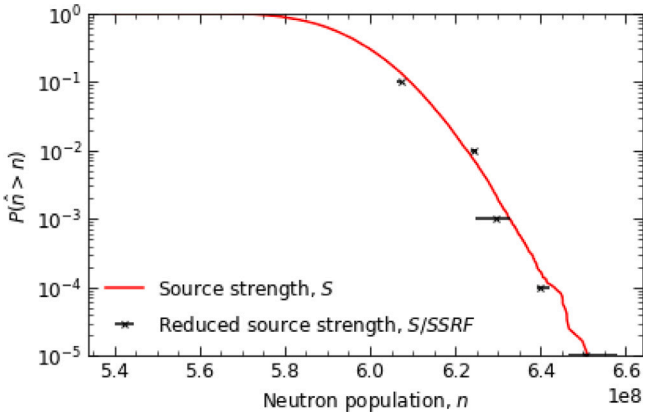

Fig. 13. The distribution in the peak neutron population for 100,000 Itô-calculus realisations for profile 3 and $\xi = 1 \times 10^{-13}$. The distribution is compared against the mean peak neutron populations calculated using the reduced source strengths $S/SSRF$ for the SSRFs at Q equal to 10^{-5}, 10^{-4}, 10^{-3}, 10^{-2}, and 10^{-1}.

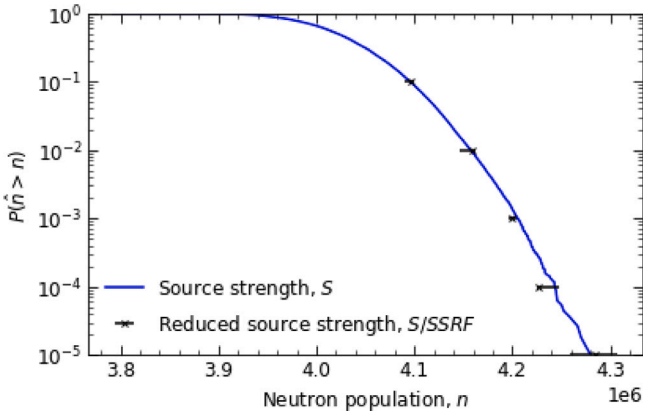

Fig. 14. The distribution in the peak neutron population for 100,000 Itô-calculus realisations for profile 4 and $\xi = 1 \times 10^{-11}$. The distribution is compared against the mean peak neutron populations calculated using the reduced source strengths $S/SSRF$ for the SSRFs at Q equal to 10^{-5}, 10^{-4}, 10^{-3}, 10^{-2}, and 10^{-1}.

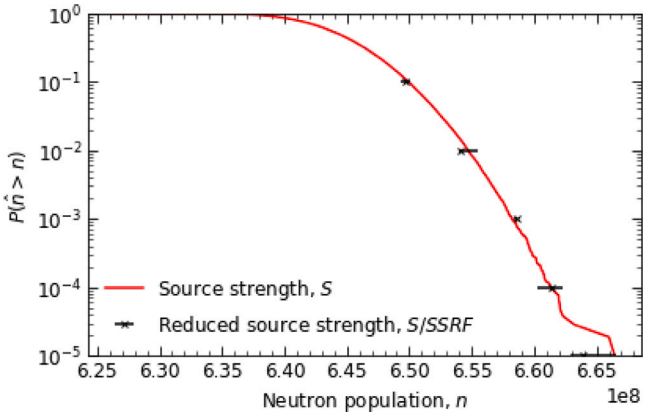

Fig. 15. The distribution in the peak neutron population for 100,000 Itô-calculus realisations for profile 4 and $\xi = 1 \times 10^{-13}$. The distribution is compared against the mean peak neutron populations calculated using the reduced source strengths $S/SSRF$ for the SSRFs at Q equal to 10^{-5}, 10^{-4}, 10^{-3}, 10^{-2}, and 10^{-1}.

$\bar{\nu}$ is the mean number of neutrons emitted during fission, and v is the neutron velocity.

The generating functions (A.1)–(A.3) and their first two derivatives with respect to z are solved by defining the final conditions (A.5)–(A.7) at time t and then solved backwards in time from $s = t$ to $s = 0$.

Equation (A.1) corresponds to the neutron population distribution at time t given the injection at earlier time s of a single neutron. Similarly, (A.2) corresponds to the delayed neutron precursor distribution at time t given the injection at earlier time s of a single delayed neutron precursor. Finally, (A.3) corresponds to the neutron population distribution at time t given the a neutron source has been present since $t = 0$.

Appendix B. Using the Pál-Bell equations to model low neutron source NPP start-up physics

The Pál-Bell equations (A.1)–(A.7) and their first two derivatives with respect to z are solved for $G_S(z,t|0)$, $G'_S(z,t|0)$, and $G''_S(z,t|0)$. Next, the saddle-point method is used to obtain properties of the neutron population CDF. The cumulative probability $Q(n^*,t|s)$, that there are fewer than n^* neutrons in the system at time t, can be calculated by solving (Williams and Eaton, 2017, 2020):

$$Q(n^*,t|s) = \frac{1}{\sqrt{2\pi\sigma_0}} \frac{G_s(z_0,t|s)}{z_0^{n^*}(1-z_0)} \tag{B.1}$$

where

$$\sigma_0 = \frac{n^*}{z_0^2} + \frac{1}{(1-z_0)^2} - \left(\frac{G'_s(z_0,t|s)}{G_s(z_0,t|s)}\right)^2 + \frac{G''_s(z_0,t|s)}{G_s(z_0,t|s)} \tag{B.2}$$

and z_0 is given as the root of the equation:

$$\frac{n^*}{z_0} = \frac{1}{(1-z_0)} + \frac{G'_s(z_0,t|s)}{G_s(z_0,t|s)}. \tag{B.3}$$

To evaluate a specific cumulative probability Q_{target} at time t, (A.1)–(A.7) are solved backwards from $s = t$ to $s = 0$ with $z = z_0$, where z_0 is an initial guess and z is bounded by 0 and 1. After solving the saddle-point equations, a certain (Q, n^*) pair will be obtained. If Q is not within a desired tolerance of Q_{target}, (A.1)–(A.7) are solved again with $z = z_1$ as a new guess. The mapping between z and (Q, n^*) is unique for each combination of system properties (neutron source strength, cross-sections, instant in time), and is unknown before solving the equations. However, the mapping is continuous between 0 and 1 which allows the correct value of z to be found by a simple bisection method.

Table C.8
Verification of the Itô-calculus implementation against results from literature for Case 1.

	Hayes and Allen (2005)	Our Implementation
$E(n(2))$	395.32	396.91
$\sigma(n(2))$	29.41	30.56
$E(c_1(2))$	300.67	300.54
$\sigma(c_1(2))$	8.36	8.11

Table C.9
Verification of the Itô-calculus implementation against results from literature for Case 2.

	Hayes and Allen (2005)	Our Implementation
$E(t)$	33.16	33.10
$\sigma(t)$	2.58	2.71

Table C.10
The delayed neutron precursor group data used for Cases 3-4.

Group	$\lambda_i(s)$	β_i
1	0.0127	0.000266
2	0.0317	0.001491
3	0.115	0.001316
4	0.311	0.002849
5	1.4	0.000896
6	3.87	0.000182

Table C.11
Verification of the Itô-calculus implementation against results from literature for Case 3.

	Hayes and Allen (2005)	Our Implementation
$E(n(0.1))$	186.31	184.39
$\sigma(n(0.1))$	164.16	164.03
$E(c_1(0.1))$	4.491×10^5	4.492×10^5
$\sigma(c_1(0.1))$	1917.2	1922.5

Appendix C. Verification of the mean and standard deviation against existing benchmarks

The mean and standard deviation of the neutron and delayed neutron precursor populations are computed using the Itô-calculus approach for a series of existing benchmark cases.

Case 1

The first case is a simple one delayed neutron precursor group model. The neutronic parameters are: $\lambda_1 = 0.1$, $\beta = \beta_1 = 0.05$, $\bar{\nu} = 2.5$, $S = 200$, $l = \frac{2}{3}$, $\rho(t) = -\frac{1}{3}$, $\vec{x}(0) = [400, 300]^T$, $h = 0.05$. 5000 realisations were computed to match the simulation conditions from literature. Table C.8 compares the mean and standard deviation in the particle populations.

Case 2

Next, the time taken for the neutron population to exceed 4000 is calculated. The neutronic parameters are: $\lambda_1 = 0.1$, $\beta = \beta_1 = 0.05$, $\bar{\nu} = 2.5$, $S = 200$, $l = 0.499002$, $\rho(t) = 0.001996$, $\vec{x}(0) = [0, 0]^T$, $h = 0.05$. The mean and standard deviation of 5000 realisations is shown in Table C.9.

Case 3

The third case models six groups of delayed neutron precursors. The neutronic parameters are: $\beta = 0.07$, $\bar{\nu} = 2.5$, $S = 0$, $l = 0.00002$, $\rho(t) = 0.003$, $\vec{x}(0) = 100 * [1, \frac{\beta_1}{\lambda_1 l}, \frac{\beta_2}{\lambda_2 l}, \ldots]^T$, with the delayed neutron precursor data shown in Table C.10. The mean and standard deviation of 5000 realisations is shown in Table C.11.

Case 4

Lastly, the mean and standard deviation in the particle populations are calculated for the following neutronic parameters: $\beta = 0.07$, $\bar{\nu} = 2.5$, $S = 0$, $l = 0.00002$, $\rho(t) = 0.007$, $\vec{x}(0) = 100 * [1, \frac{\beta_1}{\lambda_1 l}, \frac{\beta_2}{\lambda_2 l}, \ldots]^T$, with the delayed neutron precursor data shown in Table C.10.

Table C.12
Verification of the Itô-calculus implementation against results from literature for Case 4.

	Hayes and Allen (2005)	Our Implementation
$E(n(0.001))$	134.55	134.82
$\sigma(n(0.001))$	91.242	94.188
$E(c_1(0.001))$	4.464×10^5	4.464×10^5
$\sigma(c_1(0.001))$	19.444	19.694

The results show good agreement between the Itô-calculus implementation used in this study and the results from literature (see Table C.11 and Table C.12).

References

Aboanber, A.E., Nahla, A.A., 2002. Generalization of the analytical inversion method for the solution of the point kinetics equations. J. Phys. A: Math. Gen. 35 (14), 3245–3263. http://dx.doi.org/10.1088/0305-4470/35/14/307.

Allen, E.J., 2007. Modelling with Itó Stochastic Differential Equations. Springer.

Allen, E.J., 2010. Stochastic difference equation and a stochastic partial differential equation of neutron transport. J. Difference Equ. Appl. 18, 1267–1285.

Authier, N., Richard, B., Humbert, P., 2014. Initiation of persistent fission chains in the fast burst reactor caliban. Nucl. Sci. Eng. 177 (2), 169–183.

Bell, G.I., 1965. On the stochastic theory of neutron transport. Nucl. Sci. Eng. 21, 390–401. http://dx.doi.org/10.13182/NSE65-1.

Bell, G.I., Anderson, W.A., Galbraith, D., 1963. Probability distribution of neutrons and precursors in multiplying medium, ll. Nucl. Sci. Eng. 16, 118–123. http://dx.doi.org/10.13182/NSE63-2.

Boland, J., 1970. Nuclear Reactor Instrumentation (In-Core) An AEC monograph. Gordon and Breach, Science Publishers, Inc.

Cooling, C.M., Williams, M.M.R., Eaton, M.D., 2016. Coupled probabilistic and point kinetics modelling of fast pulses in nuclear systems. Ann. Nucl. Energy 94, 655–671. http://dx.doi.org/10.1016/j.anucene.2016.04.012.

Cooling, C.M., Williams, M.M.R., Eaton, M.D., 2018. CALLISTO-SPK: A stochastic point kinetics code for performing low source nuclear power plant start-up and power ascension calculations. Ann. Nucl. Energy 113, 319–331. http://dx.doi.org/10.1016/j.anucene.2017.11.022.

da Silva, M.W., Vasques, R., Bodmann, B., Vilhena, M., 2016. A nonstiff solution for the stochastic neutron point kinetics equations. Ann. Nucl. Energy 97, 47–52. http://dx.doi.org/10.1016/j.anucene.2016.06.026.

Gang, X., 2011. The simulation of probability distribution of the burst waiting time of neutron initiation. Nucl. Sci. Eng. 169, 56–67.

Hannauer, S., 1963. Role of Neutron Source in Reactor Safety. Nuclear Safety 4, 52–55.

Harrer, J.M., 1963. Nuclear Reactor Control Engineering. D. Van Nostrand Company Inc.

Harrer, J.M., Beckerley, J.G., 1973. Nuclear Power Reactor Instrumentation Systems Handbook, vol. 1, Technical Information Center.

Harrer, J.M., Beckerley, J.G., 1974. Nuclear Power Reactor Instrumentation Systems Handbook, vol. 2, Technical Information Center.

Harris, D.R., 1958. Stochastic Fluctuations in a Power Reactor. Technical Repor, WAPD-TM-190 Bettis Atomic Power Division, http://dx.doi.org/10.2172/4250011.

Harris, D.R., 1964. Naval Reactors Physics Handbook Vol I, Selected Basic Techniques, A. Radkowsky, Ed. United States Atomic Energy Commission, http://dx.doi.org/10.2172/4007148.

Hayes, J.G., Allen, E.J., 2005. Stochastic point-kinetics equations in nuclear reactor dynamics. Ann. Nucl. Energy 32, 572–587.

Humbert, P., Méchitoua, B., 2004. Simulation of caliban reactor burst wait time and initiation probability using a point reactor model and PANDA code. In: Proceedings of the PHYSOR 2004: The Physics of Fuel Cycles and Advanced Nuclear Systems - Global Developments.

Hurwitz, Jr., H., 1959. Approximate analysis of reactor start-up incidents. Nucl. Sci. Eng. 6, 11–17. http://dx.doi.org/10.13182/NSE59-A25620.

Hurwitz, Jr., H., Macmillan, D.B., Smith, J.H., Storm, M.L., 1963a. Kinetics of low source reactor startups. Part I. Nucl. Sci. Eng. 15, 166–186. http://dx.doi.org/10.13182/NSE63-3.

Hurwitz, Jr., H., Macmillan, D.B., Smith, J.H., Storm, M.L., 1963b. Kinetics of low source reactor startups. Part II. Nucl. Sci. Eng. 15, 187–196. http://dx.doi.org/10.13182/NSE63-4.

Lewis, E.E., 1977. Nuclear Power Reactor Safety. John Wiley & Sons, Ltd.

MacMillan, D., 1970. Probability distribution of neutron populations in a multiplying assembly. Nucl. Sci. Eng. 39, 329–336.

MacMillan, D.B., Storm, M.L., 1963. Kinetics of Low Source Reactor Startups - Part III. Nucl. Sci. Eng. 16 (4), 369–380. http://dx.doi.org/10.13182/NSE63-A26547.

Martin, R.C., Knauer, J.B., Balo, P.A., 2000. Production, distribution and applications of Californium-252 neutron sources. Appl. Radiat. Isot. 53, 785–792. http://dx.doi.org/10.1016/S0969-8043(00)00214-1.

Nahla, A.A., 2017. Stochastic model for the nonlinear point reactor kinetics equations in the presence Newtonian temperature feedback effects. J. Difference Equ. Appl. 23 (6), 1003–1016. http://dx.doi.org/10.1080/10236198.2017.1308507.

Pál, L., 1958. Statistical fluctuations of neutron multiplication. Magyar Tudomanyos Akad. Kozponti Fiz. Kutato Intezetenek Kozlemenyei 6.

Pál, L., 1961a. Statistical Theory of the Chain Reaction in Nuclear Reactors I. Central Scientific Research Institutue for Physics of the Hungarian Academy of Science.

Pál, L., 1961b. Statistical Theory of the Chain Reaction in Nuclear Reactors II. Central Scientific Research Institutue for Physics of the Hungarian Academy of Science.

Pál, L., 1961c. Statistical Theory of the Chain Reaction in Nuclear Reactors III. Central Scientific Research Institutue for Physics of the Hungarian Academy of Science.

Pázsit, I., Pál, L., 2007. Neutron Fluctuations. Elsevier Science, http://dx.doi.org/10.1016/B978-0-08-045064-3.X5001-7.

Saha Ray, S., Patra, A., 2013. Numerical solution of fractional stochastic neutron point kinetic equation for nuclear reactor dynamics. Ann. Nucl. Energy 54, 154–161. http://dx.doi.org/10.1016/j.anucene.2012.11.007.

Schultz, M.A., 1955. Control of Nuclear Reactors and Power Plants. McGraw Hill.

Shaw, J., 1969. Reactor Operation. Pergamon Press.

Shimazaki, Y., Sawahata, H., Shinohara, M., Yanagida, Y., Kawamoto, T., Takada, S., 2016. Improvement of neutron startup source handling work by developing new transportation container for high-temperature engineering test reactor (HTTR). J. Nucl. Sci. Technol. 54 (2), 260–266. http://dx.doi.org/10.1080/00223131.2016.1255574.

Suescun-Diaz, D., Oviedo-Toress, Y.M., Giron-Cruz, L.E., 2018. Solution of the stochastic point kinetics equations using the implicit Euler-Maruyama method. Ann. Nucl. Energy 117, 45–52. http://dx.doi.org/10.1016/j.anucene.2018.03.013.

Sutton, T.M., LaCharite, A.D., Prinja, A.K., 2017. Marduk : A Monte Carlo code for analyzing stochastic neutron population dynamics. URL https://api.semanticscholar.org/CorpusID:165162296.

Tucker, C., 2019. How to Drive a Nuclear Reactor. Springer, http://dx.doi.org/10.1007/978-3-030-33876-3.

Williams, M.M.R., 1974. Random processes in nuclear reactors. Pergamon Press, http://dx.doi.org/10.1109/TNS.1975.4328076.

Williams, M.M.R., 2017. Burst wait-times in the caliban reactor using the Gamma probability distribution function. Nucl. Sci. Eng. 183 (1), 116–125. http://dx.doi.org/10.13182/NSE15-62.

Williams, M.M.R., 2020. ADDENDUM: Approximate methods for inverting generating functions from the Pál-Bell equations for low source problems. Nucl. Sci. Eng. 194, 84–85. http://dx.doi.org/10.1080/00295639.2019.1687193.

Williams, M.M.R., 2023. The relationship between the backward and forward equations of stochastic neutron transport and associated matters. Ann. Nucl. Energy 186, 109746. http://dx.doi.org/10.1016/j.anucene.2023.109746.

Williams, M.M.R., Eaton, M.D., 2017. A theory of low source start-up based on the Pál-Bell equations. Ann. Nucl. Energy 102, 317–348. http://dx.doi.org/10.1016/j.anucene.2016.12.014.

Williams, M.M.R., Eaton, M.D., 2018. Spatial effects in low neutron source start-up and associated stochastic phenomena. Ann. Nucl. Energy 111, 616–634. http://dx.doi.org/10.1016/j.anucene.2017.09.015.

Williams, M.M.R., Eaton, M.D., 2020. Corrigendum to paper: A theory of low source startup based on the Pál-Bell equations [ann nucl energy 102 (2017) 317].. Ann. Nucl. Energy 140, 107061. http://dx.doi.org/10.1016/j.anucene.2019.107061.